HHS Public Access

Author manuscript

J Am Chem Soc. Author manuscript; available in PMC 2017 December 01.

Published in final edited form as:

J Am Chem Soc. 2017 October 18; 139(41): 14372–14375. doi:10.1021/jacs.7b08161.

Achieving One-Electron Oxidation of a Mononuclear Nonheme Iron(V)-Imido Complex

Seungwoo Hong[†,‡,#], **Xiaoyan Lu**[†,#], **Yong-Min Lee**[†], **Mi Sook Seo**[†], **Takehiro Ohta**[±], **Takashi Ogura**[±,⊥], **Martin Clémancey**[‖], **Pascale Maldivi**[§,*], **Jean-Marc Latour**[*,‖], **Ritimukta Sarangi**[¶,*], and **Wonwoo Nam**[†,*,&]

[†]Department of Chemistry and Nano Science, Ewha Womans University, Seoul 03760, Korea

[‡]Department of Chemistry, Sookmyung Women's University, Seoul 04310, Korea

[±]Picobiology Institute, Graduate School of Life Science, University of Hyogo, RSC-UH LP Center, Hyogo 679-5148, Japan

[‖]LCBM/PMB and CEA/BIG/CBM/and CNRS UMR 5249, Université Grenoble Alpes, Grenoble 38054, France

[§]CEA, CNRS, INAC, SYMMES, Université Grenoble Alpes, Grenoble 38000, France

[¶]Stanford Synchrotron Radiation Lightsource, SLAC National Accelerator Laboratory, California 94025, United States

[&]State Key Laboratory for Oxo Synthesis and Selective Oxidation, Lanzhou Institute of Chemical Physics, Chinese Academy of Sciences, Lanzhou 730000, China

Abstract

A mononuclear nonheme iron(V)-imido complex bearing a tetraamido macrocyclic ligand (TAML), $[Fe^{V}(NTs)(TAML)]^{-}$ (**1**), was oxidized by one-electron oxidants, affording formation of an iron(V)-imido TAML cation radical species, $[Fe^{V}(NTs)(TAML^{+\bullet})]$ (**2**); **2** is a diamagnetic (S = 0) complex, resulting from the antiferromagnetic coupling of the low-spin iron(V) ion (S = 1/2) with the one-electron oxidized ligand ($TAML^{+\bullet}$). **2** is a competent oxidant in C–H bond functionalization and nitrene transfer reaction, showing that the reactivity of **2** is greater than that of **1**.

[*]Corresponding Authors: wwnam@ewha.ac.kr, ritis@slac.stanford.edu, jean-marc.latour@cea.fr, pascale.maldivi@cea.fr.
[#]S.H. and X.L. contributed equally to this work.
[⊥]Deceased author.

ORCID

Seungwoo Hong: 0000-0001-7953-8433
Yong-Min Lee: 0000-0002-5553-1453
Wonwoo Nam: 0000-0001-8592-4867

Notes

The authors declare no competing financial interest.

Supporting Information

The Supporting Information is available free of charge on the ACS Publications website at DOI: 10.1021/jacs.7b08161.
Experimental Section, Tables S1–S8, and Figures S1–S24 (PDF)

High-valentiron-oxo and -imido species have been invoked as key intermediates in enzymatic and synthetic oxidative transformation reactions.[14] In biomimetic studies, heme and nonheme iron-oxo complexes have been synthesized, characterized, and investigated in various oxidation reactions over the past several decades.[2,3] Compared to the heme and nonheme iron-oxo species, the chemistry of iron-imido analogs is less clearly understood. Moreover, unlike the iron(IV and V)-oxo systems, most of the synthetic iron-imido complexes reported so far are limited to iron(IV)-imido complexes,[5] and a mononuclear iron(V)-imido complex bearing a highly negatively charged TAML, $[Fe^{V}(NTs)(TAML)]^{-}$ (**1**), was successfully synthesized by some of us very recently.[6] Encouraged by the successful synthesis of **1**, we attempted to oxidize it further to obtain a species such as $[Fe^{VI}(NTs)\text{-}(TAML)]$. Interestingly, we observed that the iron(V)-imido complex was oxidized at the TAML site, but not at the iron center. Herein, we report for the first time the synthesis, spectroscopic characterization, and reactivity studies of a novel iron(V)-imido TAML cation radical species, $[Fe^{V}(NTs)\text{-}(TAML^{+\bullet})]$ (**2**) (see Scheme 1).

The iron(V)-imido TAML complex, $[Fe^{V}(NTs)(TAML)]^{-}$ (**1**), was synthesized by following reported procedures (see Experimental Section in Supporting Information (SI)).[6] The cyclic voltammogram of **1** exhibited one reversible wave centered at 0.86 V vs SCE in CH_3CN, with the reduction and oxidation peak potentials at 0.82 and 0.90 V, respectively (SI, Figure S1). Given the electrochemical property of **1**, the oxidation of **1** was performed with one-electron oxidants, such as $[Fe^{III}(bpy)_3]^{3+}$ (E_{ox} = 1.06 V vs SCE), tris(4-bromophenyl)-ammoniumyl hexachloroantimonate, $[(4\text{-}BrC_6H_4)_3N]SbCl_6$ (TBPA, E_{ox} = 1.08 V vs SCE), and $[Ru^{III}(bpy)_3]^{3+}$ (E_{ox} = 1.24 V vs SCE).[7] Addition of the oxidants to the CH_3CN solution of **1** at −40 °C immediately changed the solution color from dark green to deep brown (SI, Experimental Section). The intermediate, denoted as **2**, was metastable ($t_{1/2}$ ~ 4 h) at −40 °C, allowing us to characterize it using various spectroscopic techniques, such as UV–vis, cold spray time-of-fiight mass spectrometry (CSI MS), electron paramagnetic resonance (EPR), resonance Raman (rRaman), nuclear magnetic resonance (NMR), Mössbauer, and X-ray absorption spectroscopy/extended X-ray absorption fine structure (XAS/EXAFS), along with density functional theory (DFT) calculations.

The UV–vis spectrum of **2** exhibited two distinct absorption bands at 545 nm (ε = 10 000 M^{-1} cm^{-1}) and 750 nm (ε = 4000 M^{-1} cm^{-1}) (Figure 1a and SI, Figure S2). Titration experiments, monitored at 750 nm as a function of the amount of $[Ru(bpy)_3]^{3+}$ added (Figure 1a, inset), indicated that the complete conversion of **1** to **2** required a stoichiometric amount of the $[Ru(bpy)_3]^{3+}$ oxidant. While the X-band EPR spectrum of **1** exhibited an isotropic signal at g = 2.00,[6] **2** is EPR silent (SI, Figure S3). The latter result suggests that (i) a low-spin (S = 1/2) iron(V) in **1** was oxidized to iron(VI) (S = 0) or (ii) a one-electron oxidized TAML was antiferromagnetically or ferromagnetically coupled with (S = 1/2) iron(V) (vide infra). CSI MS of **2** in positive mode revealed two prominent ion peaks at m/z of 618.1 and 659.2, with mass and isotope distribution patterns corresponding to $\{Na[Fe(NTs)\text{-}(TAML)]\}^{+}$ (calculated m/z of 618.1) and $\{Na[Fe(NTs)\text{-}(TAML)(CH_3CN)]\}^{+}$ (calculated m/z of 659.1), respectively (SI, Figure S4). When **2** was generated with ^{15}N-labeled **1**, which was synthesized using $PhI^{15}NTs$, one-mass unit shift from m/z of 618.1 to 619.1 and from m/z of 659.2 to 660.2 was observed. The latter result demonstrates that **2**

contains one NTs group (SI, Figure S4). The rRaman spectrum of **2**, upon 441.6 nm-excitation in CH_3CN at −40 °C, exhibited an isotopically sensitive doublet feature centered at 796 cm^{-1}, which shifted to a new doublet centered at 770 cm^{-1} upon ^{15}N-labeling of **2** (**2**-^{15}NTs; SI, Figure S5). The isotopic shift of 26 cm^{-1} is in good agreement with the calculated value of 21 cm^{-1} for a diatomic Fe–N oscillator (Hooke's Law). It is notable that the rRaman spectrum of **1** showed a Fe–N stretching vibration at 817 cm^{-1} with a doublet feature,[6] which is ~20 cm^{-1} higher than that of **2** (vide infra). ^{1}H NMR and 2D ^{1}H–^{1}H COSY experiments were performed in CD_3CN at −40 °C (SI, Figures S6–S8). All peaks in the ^{1}H NMR spectra (SI, Figure S6) were in the diamagnetic region, indicating that **2** is a diamagnetic species ($S = 0$).

Mössbauer spectra of **2** were collected at 4.2 K using fields of 0, 4, and 7 T applied parallel to the γ-ray (Figure 1b). In the absence of applied field, the spectrum consists of a quadrupole doublet centered at $\delta = -0.34$ mm s^{-1} with a quadrupole splitting of $\Delta E_Q = 3.62$ mm s^{-1}. These parameters are very similar to those of **1** ($\delta = -0.40$ mm s^{-1}, $\Delta E_Q = 3.83$ mm s^{-1}),[6] suggesting that the Fe ions in **1** and **2** have the same oxidation state. Application of a magnetic field splits the doublet, but the whole spectrum stays confined to a narrow range (−2 to +2 mm s^{-1}), indicating that **2** possesses an overall spin of $S = 0$ and the set of three spectra could be simulated perfectly under this assumption. Thus, the Mössbauer data suggest that the electronic structure of **2** is best described as a low-spin ($S = 1/2$) iron(V) center antiferromagnetically coupled to a radical spin located on the ligand.

Fe K-edge XAS data on solution samples of **1** and **2** are presented in Figure 2a. The data show very little difference in the rising-edge energy or pre-edge energy position, indicating no change in the oxidation state of the Fe centers in **1** and **2**, as shown in the Mössbauer study. The Fe K-pre-edge intensity is a sensitive probe of the Fe–N bond distance. This is because the short Fe–N bond is along the molecular z-axis, which leads to a strong Fe $3d_{z^2}$–$4p_z$ mixing, which increases with the increase in distortion along the Fe–N bond (i.e., shortening of the Fe–N bond).[8,9] The very small difference in the two pre-edge intensities indicates that the bond distances are not dramatically different in **1** and **2**. To confirm this structural assessment, EXAFS data were measured on **1** and **2** and a comparison is shown in Figure 2b and SI, Figure S9. A qualitative comparison shows very similar structures for **1** and **2**, with loss of long-range multiple scattering at high R (R' ~ 3–4 Å) in **2** relative to **1**. This is consistent with perturbation in TAML due to oxidation. FEFF fits for **2** indicate that the data are consistent with a first shell with 1 Fe–N at 1.66 Å and 4 Fe–N at 1.85 Å. The second shell was fit with single and multiple scattering contributions from TAML. No long distance shell (between R' ~ 3–4 Å) was observed. For comparison, the EXAFS data for **1** were also fit using the same protocol used here and the best fit was obtained using 1 Fe–N at 1.67 Å and 4 Fe–N 1.86 Å. It is important to note that the EXAFS resolution is ±0.02 Å, indicating that the first-shell structures of **1** and **2** are very similar. Interestingly, however, a difference in intensity in the Fourier transforms at high R is observed, which is replicated over several measurements. This indicates a change in TAML due to oxidation. Multiple-scattering components from the outer edge of TAML were required to obtain a good fit to **1** (SI, Table S1), suggesting that the TAML ring in **1** is oriented in such a way as to maximize this longer-range contribution to the EXAFS. This typically occurs when the ring is more

ordered or planar. Thus, the XAS/EXAFS data indicate that the oxidation of **1** occurs on TAML, not at the Fe center.

Insight into the electronic structure of **2** was gained from DFT calculations (SI, Figure S10). Relying on the EXAFS and Mössbauer experiments, the hybrid B3LYP* with a decreased contribution of exact exchange (15%),[10] compared to the well-known B3LYP functional (20%), proved to yield a satisfactory agreement with experiment (SI, Table S2). A singlet ground state was observed, with structural parameters in good agreement with EXAFS data, with a Fe-NTs distance of 1.68 Å and an averaged Fe–N (TAML) distance of 1.88 Å. The calculated Mössbauer parameters are also consistent with experiment, with ΔE_Q = 3.49 mm s^{-1} (exp. 3.62 mm s^{-1}) and δ = −0.30 mm s^{-1} (exp. −0.34 mm s^{-1}). The group spin densities unambiguously identify this electronic structure as being a low-spin Fe^V ion antiferromagnetically coupled to a radical on TAML (SI, Table S3). A plot of the spin densities shows that the latter radical is localized on the o-phenylenediamine part, as a result of its conjugated character (SI, Figure S11). Finally, the Kohn–Sham orbital diagram of this Fe^V(NTs) TAML cation radical species is fully consistent with the picture described above (SI, Table S4). The Fe electronic configuration is $d_{xy}^2 d_{xz}^{\alpha 1}$ corresponding to a Fe^V low-spin ion. The LUMO is localized on the α N (p_z) orbitals of the *o*-phenylenediamine part of TAML, resulting in a negative spin density on TAML (SI, Figure S12). Such a radical character on TAML site in high-valent transition metal TAML complexes was previously discussed in theoretical studies.[11] Notably, the Fe^{VI} d^2 configuration could be obtained as a very low-lying excited state, but the resulting structural and Mössbauer parameters are not consistent with experiments. On the basis of the spectroscopic characterization and DFT calculations, we conclude that an iron(V)-imido TAML cation radical complex, [Fe^V(NTs)($TAML^{+\bullet}$)] (**2**), was formed in one-electron oxidation of the iron(V)-imido TAML complex, [Fe^V(NTs)-(TAML)]$^-$ (**1**).

The reactivity of **2** was investigated in C–H bond functionalization and nitrene transfer reaction and then compared with that of **1**. Upon addition of xanthene to a CH_3CN solution of **2**, absorption bands at 545 and 750 nm disappeared, and the decay rate increased proportionally with the increase of xanthene concentration (SI, Figure S13); a second-order rate constant (k_2) of 1.3(2) × 10 M^{-1} s^{-1} at 15 °C was determined. This k_2 value of **2** was slightly greater (~2.5 times) than that of **1** (e.g., 4.7 M^{-1} s^{-1} at 15 °C).[6] A kinetic isotope effect (KIE) value of 7(1) was obtained in the xanthene oxidation by **2** (SI, Figure S14 and Table S5); a KIE value of 11(1) was reported in the oxidation of xanthene by **1**.[6] We also determined the k_2 values in the oxidation of other substrates, such as 9,10-dihydroanthracene (DHA), indene, and fluorene (SI, Figure S15 and Table S5), and a linear correlation between the k_2 values and the C–H bond dissociation energies (BDEs) of substrates was observed (Figure 3a). The observation of a large KIE value and a good correlation between the reaction rates and the C–H BDEs of substrates leads us to conclude that a hydrogen atom (H atom) abstraction from the C–H bonds of substrates by **2** is the rate-determining step.

Product analysis of the xanthene and fluorene oxidation by **2** revealed the formation of xanthene-NHTs and fluorene-NHTs as major products (~90% yield in both cases). We also found the formation of [Fe^{IV}(TAML)] as the decay product of **2**; [Fe^{IV}(TAML)] was synthesized independently as an authentic sample to compare the spectroscopic data of the

decay product of **2** (SI, Figures S16–S19). Taken together, the amination reaction by **2** occurs via a H atom abstraction of substrates to give aminated products and [Fe^{IV}(TAML)] as the decay product of **2**.

In the nitrene transfer reaction by **2**, *para*-X-substituted thioanisoles (X = OMe, Me, H, Cl, and CN) were used as substrates under stopped-flow kinetic conditions at −40 °C. In the sulfimidation of thioanisole by **2**, a k_2 value of 3.3(2) × 10 M^{-1} s^{-1} was determined at −40 °C, which was then calculated to be 4.4 × 10^2 M^{-1} s^{-1} at 15 °C (SI, Figures S20 and S21). By comparing the k_2 values of **1** and **2**, we found that the reactivity of the iron(V)-imido complex was markedly enhanced (over 10^4 folds) by the one-electron oxidation of the supporting ligand (e.g., 2.6 × 10^{-2} M^{-1} s^{-1} for **1** versus 4.4 × 10^2 M^{-1} s^{-1} for **2**).[6] The analysis of the reaction solution revealed the formation of PhS(=NTs)CH_3 (~95% yield) and [Fe^{IV}(TAML)] as products (SI, Figures S22 and S23). In addition, as often proposed in the sulfoxidation of thioanisoles by high-valent metal-oxo species,[12] a large negative slope of −9.1, which was obtained by plotting log k_2 values against one-electron oxidation potentials (E_{ox}) of *para*-X-substituted thioanisoles (Figure 3b; SI, Figure S24 and Table S6), suggests that the sulfimidation of thioanisoles by **2** proceeds via electron transfer, followed by nitrene transfer.

In order to reconcile the reactivity differences of **1** and **2** in the amination and sulfimidation reactions, we calculated their H atom affinity (HAA) for aminations and electron affinity (EA) for sulfimidation (SI, Table S7). The EAs for **1** and **2** are 103.9 and 122.8 kcal mol^{-1}, respectively, a trend which is in line with the experimental results obtained in the sulfimidation of thioanisole by **1** and **2**. The calculated HAAs of **1** and **2** for the amination reactivity were found to be very close, being 81.9 and 85.2 kcal mol^{-1}, respectively, which is consistent with their similar reactivity in the amination reactions. The group spin densities of **1**–H and **2**–H show a similar Fe^{IV}-NHTs configuration (SI, Table S8), explaining the closeness of their HAAs.

In summary, an iron(V)-imido TAML cation radical complex, [Fe^{V}(NTs)($TAML^{+\bullet}$)] (**2**), was synthesized for the first time by oxidizing an iron(V)-imido TAML complex, [Fe^{V}(NTs)(TAML)]$^-$ (**1**), with one-electron oxidants; **2** can be considered formally as an iron(VI)-imido species as Cpd I is considered formally as an iron(V)-oxo species in heme systems.[3] The one-electron oxidized species, **2**, showed slightly increased reactivity in amination reaction (i.e., ~2.5 times increase) but markedly enhanced reactivity in nitrene transfer reaction (i.e., ~17 000 times increase). Future studies will focus on detailed mechanisms and reactivity comparison of **1** and **2** in various oxidation reactions.

Supplementary Material

Refer to Web version on PubMed Central for supplementary material.

Acknowledgments

This work was supported by NRF of Korea through CRI (NRF-2012R1A3A2048842 to W.N.), GRL (NRF-2010-00353 to W.N.), Basic Science Research Program (2017R1D1A1B03029982 to Y.M.L.), and MSIP (NRF-2017R1C1B2002037 to S.H.). T.O. acknowledges the support of Grant-in-Aid for Scientific Research (No. 15H00960) by JSPS. J.-M.L. and P.M. were supported by ANR (ANR-11-LABX-003) and GENCI-IDRIS (Grant

2017-A0020807648). XAS data were measured at SSRL and R.S. was supported by NIH P41 grant (P41GM103393) and DOE-BER.

References

1. (a) Krebs C, Fujimori DG, Walsh CT, Bollinger JM Jr. Acc Chem Res. 2007; 40:484. [PubMed: 17542550] (b) Holland PL. Acc Chem Res. 2008; 41:905. [PubMed: 18646779] (c) Solomon EI, Goudarzi S, Sutherlin KD. Biochemistry. 2016; 55:6363. [PubMed: 27792301] (d) Proshlyakov DA, McCracken J, Hausinger RP. J Biol Inorg Chem. 2017; 22:367. [PubMed: 27812832]
2. (a) Nam W, Lee YM, Fukuzumi S. Acc Chem Res. 2014; 47:1146. [PubMed: 24524675] (b) Cook SA, Borovik AS. Acc Chem Res. 2015; 48:2407. [PubMed: 26181849] (c) Puri M, Que L Jr. Acc Chem Res. 2015; 48:2443. [PubMed: 26176555] (d) Engelmann X, Monte-Pérez I, Ray K. Angew Chem, Int Ed. 2016; 55:7632.
3. (a) Huang X, Groves JT. J Biol Inorg Chem. 2017; 22:185. [PubMed: 27909920] (b) Yosca TH, Ledray AP, Ngo J, Green MT. J Biol Inorg Chem. 2017; 22:209. [PubMed: 28091754]
4. (a) Eikey RA, Abu-Omar MM. Coord Chem Rev. 2003; 243:83.(b) Saouma CT, Peters JC. Coord Chem Rev. 2011; 255:920. [PubMed: 21625302] (c) Roizen JL, Harvey ME, Du Bois J. Acc Chem Res. 2012; 45:911. [PubMed: 22546004] (d) Zhang L, Deng L. Chin Sci Bull. 2012; 57:2352.(e) Ray K, Heims F, Pfaff FF. Eur J Inorg Chem. 2013; 2013:3784.
5. (a) Verma AK, Nazif TN, Achim C, Lee SC. J Am Chem Soc. 2000; 122:11013.(b) Thomas CM, Mankad NP, Peters JC. J Am Chem Soc. 2006; 128:4956. [PubMed: 16608321] (c) Bart SC, Lobkovsky E, Bill E, Chirik PJ. J Am Chem Soc. 2006; 128:5302. [PubMed: 16620076] (d) Klinker EJ, Jackson TA, Jensen MP, Stubna A, Juhász G, Bominaar EL, Münck E, Que L Jr. Angew Chem, Int Ed. 2006; 45:7394.(e) Mehn MP, Brown SD, Jenkins DM, Peters JC, Que L Jr. Inorg Chem. 2006; 45:7417. [PubMed: 16933946] (f) Leeladee P, Jameson GNL, Siegler MA, Kumar D, de Visser SP, Goldberg DP. Inorg Chem. 2013; 52:4668. [PubMed: 23527920] (g) Liu Y, Guan X, Wong ELM, Liu P, Huang JS, Che CM. J Am Chem Soc. 2013; 135:7194. [PubMed: 23634746] (h) Kumar S, Faponle AS, Barman P, Vardhaman AK, Sastri CV, Kumar D, de Visser SP. J Am Chem Soc. 2014; 136:17102. [PubMed: 25392052] (i) Wang L, Hu L, Zhang H, Chen H, Deng L. J Am Chem Soc. 2015; 137:14196. [PubMed: 26505122] (j) Iovan DA, Betley TA. J Am Chem Soc. 2016; 138:1983. [PubMed: 26788747] (k) Gouré E, Senthilnathan D, Coin G, Albrieux F, Avenier F, Dubourdeaux P, Lebrun C, Maldivi P, Latour JM. Angew Chem, Int Ed. 2017; 56:4305.(l) Bucinsky L, Breza M, Lee WT, Hickey AK, Dickie DA, Nieto I, DeGayner JA, Harris TD, Meyer K, Krzystek J, Ozarowski A, Nehrkorn J, Schnegg A, Holldack K, Herber RH, Telser J, Smith JM. Inorg Chem. 2017; 56:4751.
6. Hong S, Sutherlin KD, Vardhaman AK, Yan JJ, Park S, Lee YM, Jang S, Lu X, Ohta T, Ogura T, Solomon EI, Nam W. J Am Chem Soc. 2017; 139:8800. [PubMed: 28628312]
7. Connelly NG, Geiger WE. Chem Rev. 1996; 96:877. [PubMed: 11848774]
8. Sarangi R. Coord Chem Rev. 2013; 257:459. [PubMed: 23525635]
9. Westre TE, Kennepohl P, DeWitt JG, Hedman B, Hodgson KO, Solomon EI. J Am Chem Soc. 1997; 119:6297.
10. Reiher M, Salomon O, Hess BA. Theor Chem Acc. 2001; 107:48.
11. (a) Conradie MM, Conradie J, Ghosh A. J Inorg Biochem. 2006; 100:620. [PubMed: 16504297] (b) Popescu D-L, Chanda A, Stadler M, Tiago de Oliveira F, Ryabov AD, Münck E, Bominaar EL, Collins TJ. Coord Chem Rev. 2008; 252:2050.
12. (a) Goto Y, Matsui T, Ozaki S, Watanabe Y, Fukuzumi S. J Am Chem Soc. 1999; 121:9497.(b) Arias J, Newlands CR, Abu-Omar MM. Inorg Chem. 2001; 40:2185. [PubMed: 11304165] (c) Taki M, Itoh S, Fukuzumi S. J Am Chem Soc. 2002; 124:998. [PubMed: 11829608] (d) McPherson LD, Drees M, Khan SI, Strassner T, Abu-Omar MM. Inorg Chem. 2004; 43:4036. [PubMed: 15206886]

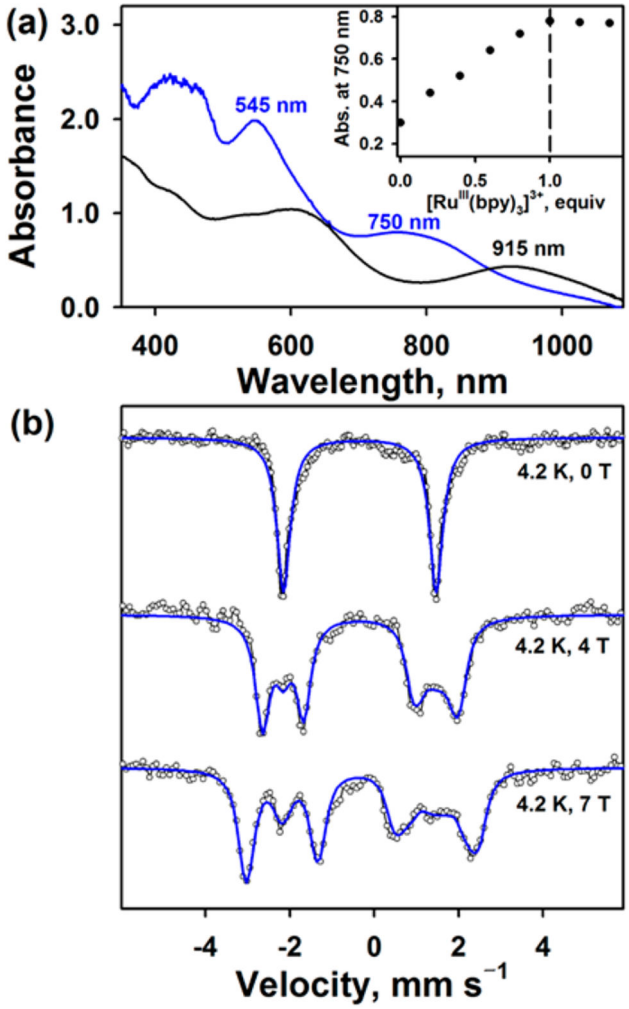

Figure 1.

(a) UV–vis spectra of $[Fe^{V}(NTs)(TAML)]^{-}$ (**1**, black line) and $[Fe^{V}(NTs)(TAML^{+\bullet})]$ (**2**, blue line); **2** was synthesized by reacting **1** (0.20 mM) with 1.0 equiv of $[Ru(bpy)_3]^{3+}$ (0.20 mM) in CH_3CN at −40 °C. Inset shows plot of the absorbance change at 750 nm due to **2** upon addition of $[Ru(bpy)_3]^{3+}$ to **1** (0.20 mM) in increment of 0.2 equiv. (b) Mössbauer spectra (black dotted lines) with fits (blue lines) for **2** recorded at 4.2 K and 0, 4, and 7 T.

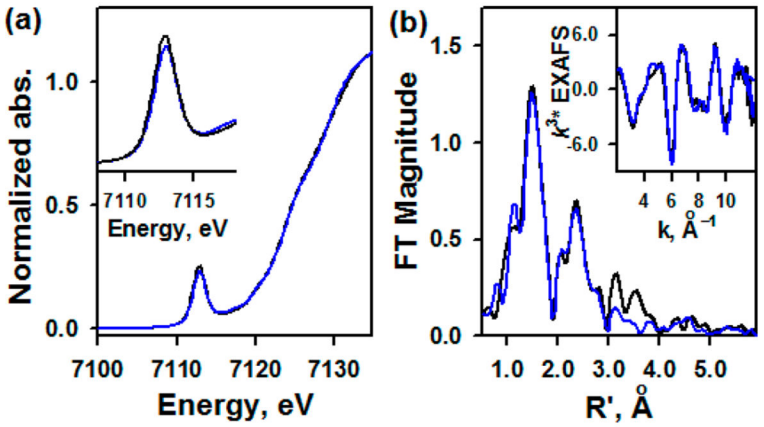

Figure 2.

(a) XAS data of **1** (black line), and **2** (blue line). Inset shows the expansion of pre-edge region. (b) Non-phase shift corrected Fourier transforms of **1** (black line) and **2** (blue line) (see SI, Figure S9).

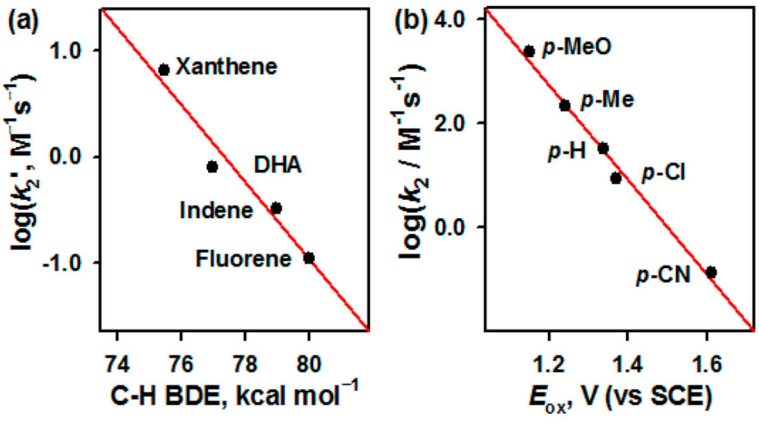

Figure 3.

(a) Plot of log k_2' against C–H BDEs of substrates in the amination reaction by **2** at 15 °C (SI, Table S5). (b) Plots of log k_2 against the E_{ox} values of *para*-X-substituted thioanisole derivatives in the sulfimidation reaction by **2** at −40 °C (SI, Table S6).

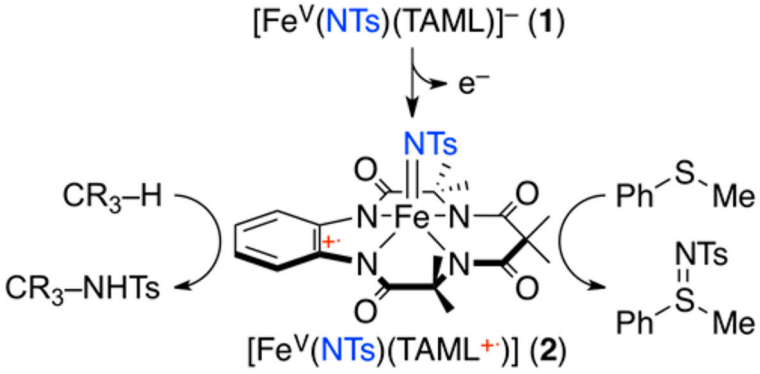

Scheme 1.
Synthesis and Reactivity of [Fe^{V}(NTs)($TAML^{+\bullet}$)]